ChemPubSoc Europe

DOI: 10.1002/chem.201703851

CHEMISTRY A European Journal Full Paper

Polyoxometalates

Polyoxometalate-Based Bottom-Up Fabrication of Graphene Quantum Dot/Manganese Vanadate Composites as Lithium Ion Battery Anodes

Yuanchun Ji,[a] Jun Hu,[b] Johannes Biskupek,[c] Ute Kaiser,[c] Yu-Fei Song,*[b] and Carsten Streb*[a]

Abstract: Lithium ion battery (LIB) electrodes require a stable connection between a redox-active metal oxide for charge storage and an electrically conductive (often carbon-based) material for charge transport. As charge transfer within the metal oxide is often a performance-limiting factor, one promising concept is the linking of charge transfer and charge storage components on the nanoscale. This would maximize the interfacial contact area and improve charging/discharging behavior. This work presents a one-step, room-temperature route giving nanostructured manganese vanadium oxide/graphene quantum dot (GQD) composite electrodes. Manganese vanadium oxide clusters are used as solution-processable precursors, which are deposited on GQDs using a sonication-driven conversion leading to electroactive, lightweight composites. Incorporation of the composites as anodes in LIBs shows high electrochemical performance featuring discharge capacities of 970 $mAh\,g^{-1}$ over 100 cycles with coulombic efficiencies near 100%. The study shows how 3d-metal oxide/GQD nanostructures can be accessed by a scalable sonication route starting from soluble, chemically tunable metal oxide clusters and graphene quantum dots.

Introduction

The efficient and stable linkage between charge storage and charge transport components is a major challenge in contemporary battery electrode design. In modern high-performance lithium ion batteries, 3d-metal oxides such as $LiCoO_2$ or $LiMn_2O_2$/$LiMnO_3$ are employed due to their relatively low weight, high energy density, and long-term stability. However, these metal oxides feature low electronic and ionic conductivity so that charge transfer between the metal current collector and the electrode material is often a major performance limitation.[1] Despite these challenges, metal oxides are promising anode materials for LIBs as they feature high redox potentials (typically in the range of 1.0–1.3 V vs. Li^+/Li) and promising specific capacities (in the order of 500 to 1200 $mAh\,g^{-1}$ for 3d-metals), leading to high theoretical specific energy densities.[2,3] To harness these benefits, new synthetic routes are required, which address the challenges in interfacing metal oxides with conductive substrates and electrolytes. One highly successful approach is the combination of nanostructured metal oxides and nanostructured carbon materials so that a maximum interfacial contact area is achieved for charge transfer.[4] Various routes have been reported that allow the deposition of nanostructured metal oxides on carbon substrates such as carbon nanotubes (CNTs) or graphene-based materials.[5–9]

Over recent years, the use of molecular metal oxides, so-called polyoxometalates (POMs),[10] for charge storage in LIBs has received significant interest, mainly based on their unique structural and electronic properties; POMs are based on redox-active, early transition metals and additional heterometals from throughout the periodic table can be introduced into their metal oxide framework.[10] Furthermore, the covalent attachment of organic functional groups to the POM anions is possible,[11] so that their reactivity as well as their linkage to carbon substrates can be tuned by chemical design.[4,12]

Thus far, mainly molybdate POMs have been employed as LIB anode materials and various covalent and non-covalent anchoring methods have been used to link them to CNTs or graphene materials.[4,13–16] In contrast, the use of the highly redox-active, lighter polyoxovanadates[17,18] in battery research has received significantly less attention, although several studies in recent years have shown their high potential as battery electrodes.[19,20] In a recent landmark study, Stimming and colleagues demonstrated the high electron storage capability of vanadium oxides and reported that the decavanadate cluster

[a] Y. Ji, Prof. Dr. C. Streb
Institute of Inorganic Chemistry I, Ulm University
Albert-Einstein-Allee 11, 89081 Ulm (Germany)
E-mail: carsten.streb@uni-ulm.de

[b] Dr. J. Hu, Prof. Dr. Y.-F. Song
State Key Laboratory of Chemical Resource Engineering
Beijing University of Chemical Technology, 100029 Beijing (P. R. China)
E-mail: songyf@mail.buct.edu.cn

[c] Dr. J. Biskupek, Prof. Dr. U. Kaiser
Central Facility of Electron Microscopy for Materials Science
Ulm (Germany)

Supporting information and the ORCID identification number(s) for the author(s) of this article can be found under https://doi.org/10.1002/chem.201703851.

$[V_{10}O_{28}]^{6-}$ can be reversibly reduced by up to ten electrons.[21] One bottleneck in current vanadate electrodes is their specific capacity, which is typically in the region of ≈250–350 mA h g^{-1}.[19–21] Thus, the development of new materials, where increased capacities are achieved by structural modification of the metal oxide or by improved interfacing between charge storage and charge transport sites, could lead to the broader usage of vanadates in lithium or post-lithium batteries.[22]

One pressing challenge in the field is the permanent immobilization of metal oxide clusters on conductive surfaces using facile means to avoid desorption and loss of electroactivity during operation.[23] One particularly promising approach is the conversion of molecular vanadium oxides into nanostructured solid-state vanadium oxides.[24,25] While this concept is established for nanostructure development,[24,25] it has thus far not been used in LIB electrode design. Thus, the merging of nanostructured vanadium oxides with graphene quantum dots can lead to high-performance electrode materials; graphene quantum dots (GQDs)[26] have attracted significant interest for nanostructured electroactive materials as they are easily accessible, feature unique electronic properties such as high electron mobility and high mechanical stability and flexibility.[26–30] The presence of functional groups (alcohols, carboxylic acids, amines, amides)[31–33] enable enhanced linkage to other materials such as metal oxides, particularly for energy storage devices.[25,34,35]

Here, for the first time, we show how redox-active, lightweight (i.e., 3d-metal based) molecular metal oxide clusters can be used as precursors for the fabrication of GQD/metal oxide composites as technologically relevant LIB anodes.

The manganese vanadate $(n\mathrm{Bu_4N})_3(\mathrm{DMA})[(\mathrm{MnCl})V_{12}O_{32}Cl]$ (= $(n\mathrm{Bu_4N})_3${**$\mathrm{MnV_{12}}$**})[36,37] was employed as a model vanadate precursor as it contains redox-active, earth-abundant manganese and vanadium centers with known activity in LIB anodes.[38–40]

Results and Discussion

The composite was prepared based on a simple ultrasonication-driven assembly method recently reported by us:[16] an aqueous dispersion of GQDs (10 mL, 30 g L^{-1})[41] and an acetonitrile solution of {**$\mathrm{MnV_{12}}$**} (20 mL, 1.0 mM)[36] were mixed and sonicated (300 W, 45 kHz) for 12 h at 25 °C. Composite **1** was recovered by centrifugation, washed three times with ethanol, and vacuum-dried (see Scheme 1). Composite **1** was obtained in yields of ca. 93 wt.% based on the total amount of precursors ({**$\mathrm{MnV_{12}}$**} and GQDs) used. The composite was fully characterized using FT-IR-, UV/Vis-, emission-, energy-dispersive X-ray and X-ray photoelectron spectroscopies, high-resolution transmission electron microscopy and thermogravimetry (for details, see below and the Supporting Information). The composite formation can also be detected by emission spectroscopy; whereas the GQDs (dispersed in water) exhibit a characteristic green-blue luminescence when irradiated with broadband UV light ($\lambda_{\mathrm{emission,\,max}}$ = 425 nm), significant emission quenching is observed upon addition of {**$\mathrm{MnV_{12}}$**} to the reaction solution (Figure 1 i).

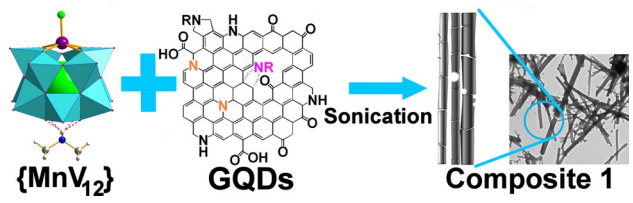

Scheme 1. Schematic illustration of the fabrication of composite **1** by sonication-driven deposition of a manganese vanadium oxide on graphene quantum dots (GQDs) using a molecular manganese vanadate ({**$\mathrm{MnV_{12}}$**}) precursor.

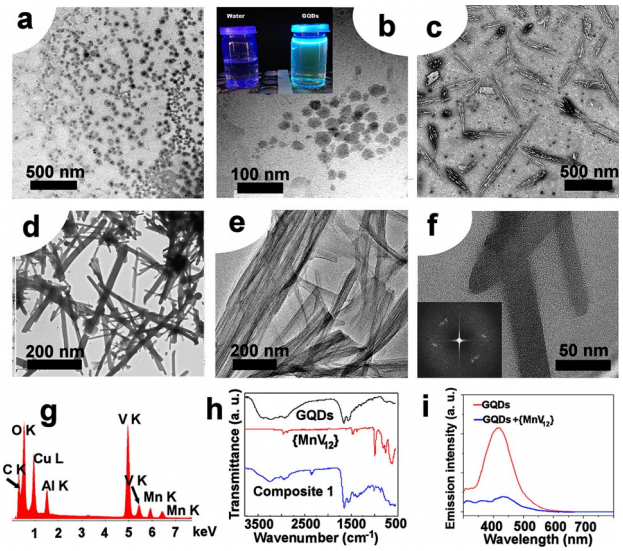

Figure 1. Characterization of composite **1**: TEM images of (a, b) graphene quantum dots (inset: luminescence of the as-prepared GQDs under broadband UV irradiation); (c) {**$\mathrm{MnV_{12}}$**} drop-cast on TEM grid; (d) composite **1**; (e, f) HRTEM of composite **1** (inset in f: Fast Fourier transform); (g) EDX spectrum of composite **1**; (h) FT-IR spectra of GQDs (black), {**$\mathrm{MnV_{12}}$**} (red), and composite **1** (blue); (i) emission spectra of GQDs in the presence and absence of {**$\mathrm{MnV_{12}}$**} in acetonitrile/water (2:1, v:v).

The nanoscale structure of the precursors and the composite were examined using high-resolution transmission electron microscopy (HRTEM). For the as-prepared GQDs, TEM shows non-aggregated, disk-shaped particles with a diameter of approx. 20 nm and a narrow size distribution (Figure 1 a, b). TEM analysis of {**$\mathrm{MnV_{12}}$**} was performed by dissolving {**$\mathrm{MnV_{12}}$**} in acetonitrile, drop-casting the solution on the TEM grid and air-drying. High-resolution TEM shows "superstructures" where several smaller rods are aligned in a co-parallel fashion to give structures up to ≈150 nm in length. Analysis of lattice fringes using Fast Fourier transforms (FFTs) of HRTEM images show layered structures with layer spacings of 0.35 nm. Composite **1** shows distinct smooth, rod-like structures with high aspect ratios (length between ≈400–800 nm, diameter between ≈30–50 nm). The analysis of FFTs of HRTEM images shows that the composite features a layered structure with layer spacings of 1.0 nm. It is suggested that the conversion between the precursor structures and the composite nanorods **1** is triggered by the energy input provided by sonication where structural

changes (e.g., delamination–realignment) of the GQDs[42] as well as structural changes of the metal oxide[16,43] could lead to the observed formation of composite **1**.

TEM-coupled energy dispersive X-ray spectroscopy (EDX) confirms that the composite contains the expected elements C, O, V, and Mn (Figure 1 g), highlighting that a true GQD/metal oxide composite is formed. Notably, the formation of the nanocomposite during synthesis can be observed by emission spectroscopy; after sonication of **{MnV_{12}}** acetonitrile solution and the strongly emitting GQDs dispersion, a significant loss of emission intensity is observed (Figure 1 i), indicating the formation of interactions between both species.[44,45] FT-IR spectroscopy of composite **1** shows the characteristic GQD vibrational modes (mainly C–C, C–N, C–O, C–H)[32] as well as metal oxide modes (mainly M–O and M–O–M (M = V, Mn))[36] (see Figure 1 h and the Supporting Information for detailed assignments).[15,46]

Thermogravimetric analysis (TGA) of GQDs, **{MnV_{12}}** and composite **1** under air flow is shown in Figure 2. The GQDs show total oxidation between 220–750 °C, in line with their composition based on C, H, O, and N, only. For **{MnV_{12}}**, a weight loss of 41.6 wt% is noted between 150–500 °C; this is in line with a loss of the organic components nBu$_4$N$^+$ and $Me_2NH_2^+$ (calcd: 38.5 wt.%) and lattice solvent.[36] Composite **1** shows a continuous weight loss between 250–550 °C with a total loss of 92.8 wt.%. This suggests that approximately 7 wt.% of **1** is composed of inorganic manganese vanadium oxides, whereas the remaining 93 wt.% are based on GQDs and organic components derived from **{MnV_{12}}**.

The chemical composition of the composite and the precursors was further analyzed using X-ray photoelectron spectroscopy (XPS). Deconvolution of the XPS data for the GQDs (Figure 3 a–c) gives four specific carbon signals (at 284.4, 285.6, 286.5, and 288.6 eV), which can be assigned to sp^2-carbon (C=C, C=N), sp^3-carbon (C–O, C–N) and oxidized C (C=O), respectively.[41] The deconvoluted N 1s spectrum features two signals at 398.6 and 401 eV, which are attributed to pyrrolic and graphitic N, respectively.[41] The deconvoluted O 1s spectrum of GQDs features three signals at 530.5, 532.0, and 533.3 eV, which are assigned to C=O, C–OH and C–O–C, respectively.[15] For **{MnV_{12}}**, XPS reveals characteristic signals for O 1s at 532.0 and 530.2 eV, Mn 2p at 641.5 eV, and V 2p at 517.2 eV (Figure 3 g and h and Figure S1 in the Supporting Information). In the composite, all signals can be observed also; however, minor shifts are observed for the N 1s and O 1s signals (typically ≈0.2–0.8 eV), which could be indicative of structural changes within the manganese vanadium oxide as well as for bonding interactions between the GQDs and the metal oxide (see below).[47] For the vanadium signal, no significant change

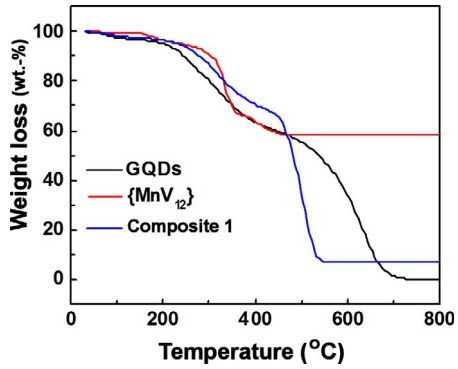

Figure 2. Thermogravimetric analysis of GQDs, **{MnV_{12}}** and composite **1**.

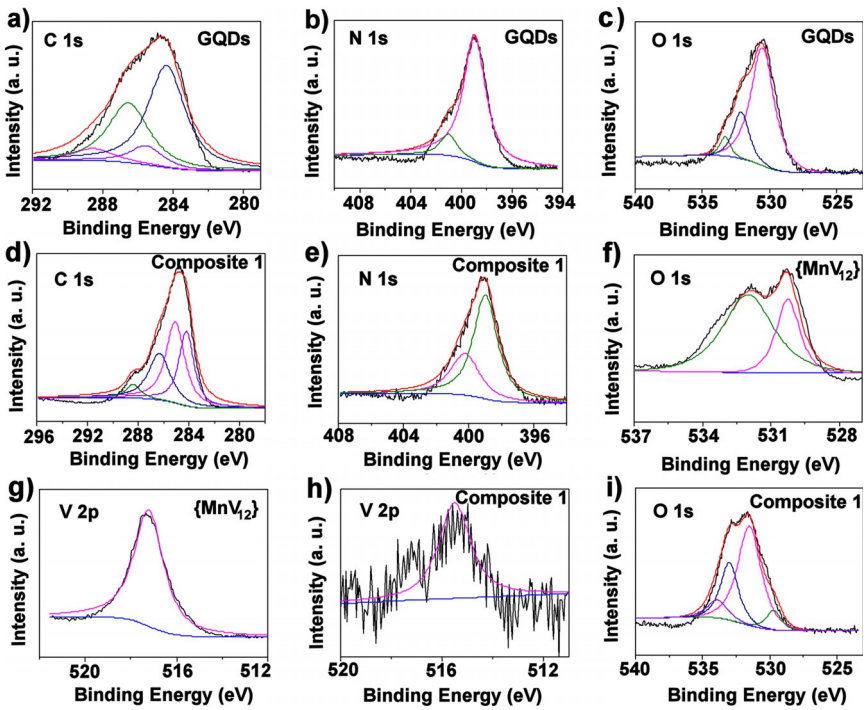

Figure 3. X-ray photoelectron spectroscopy (XPS) and deconvoluted XPS spectra of GQDs (a–c), **{MnV_{12}}** (f, g), and composite **1** (d, e, h, and i).

is observed, indicating that the chemical environment of the V does not change significantly upon composite formation. As expected, composite **1** features one additional signal in the O 1s spectrum (at 529.6 eV), which is related to the presence of the metal oxide. (Figure 3i and Figure S1).[48,49] The binding mode between the metal oxide particles and the GQDs is still under investigation and could be due to electrostatic interactions, the formation of covalent bonds (e.g., M–O–C; M = V, Mn) or supramolecular interactions such as hydrogen bonding (e.g., C–OH···O–M, M = V, Mn), or indeed a combination of these. However, purely based on the XPS and FT-IR data, no more detailed insights are possible and future studies using Raman and X-ray absorption spectroscopies (NEXAFS, XANES) will be performed to gain insights into this important question, which has implications for the battery performance discussed below.[4]

The performance of composite **1** as an anode in a coin-cell lithium ion battery was examined: to this end, coin cells were assembled in an argon-filled glove box with the anode as-fabricated (composite **1**: carbon black: poly(vinylidene fluoride), weight ratio 50:40:10), metallic lithium foil as a counter electrode, and 1.0 M $LiPF_6$ solution in ethylene carbonate (EC)/diethyl carbonate (DEC) (1:1, v:v) as electrolyte. Cyclic voltammetry of **1** (Figure 4, scan rate: 0.1 mVs^{-1}; scan range: 0.01–3 V vs. Li^+/Li) shows an irreversible reduction peak at approx. 0.7 V in the first reduction run, which indicates the formation of a solid electrolyte interface (SEI).[15] Consequently, the peak is not observed in subsequent cycles.

The reduction signal between 0.01–0.2 V is attributed to the Li^+ insertion reaction. The corresponding oxidation peak at ca. 0.2 V observed in the charging process is assigned to Li^+ extraction from composite **1**. This signal can be observed in the following cycles, suggesting that Li^+ insertion/extraction is reversible under the given experimental conditions. Two additional redox transitions are observed in the 2nd and 3rd cycle. The process at $E_{red} = 0.99$ V/$E_{ox} = 1.17$ V is tentatively assigned to the $V^{V/IV}$ redox couple, whereas the weak signal at $E_{red} = 1.85$ V/$E_{ox} = 2.36$ V is tentatively assigned to the $Mn^{III/II}$ couple (Supporting Information, Figure S2).[36] Figure 4b shows the first three charge–discharge cycles of composite **1** at a current density of 100 $mA\,g^{-1}$. The first discharge capacity is 1645 $mA\,g^{-1}$ and is reduced to 985 $mA\,g^{-1}$ in the third cycle. Over subsequent cycles, the specific capacity stabilizes at ca. 970 $mA\,g^{-1}$ (Figure 5). As described above, this behavior is assigned to the formation of a solid-electrolyte interface (SEI).[15]

The rate performance of composite **1** was evaluated at current densities between 50 $mA\,g^{-1}$ and 2000 $mA\,g^{-1}$ at voltages between 0–3.0 V vs. Li^+/Li. (Figure 5a). As expected, higher current densities result in lower charge and discharge capacities; for example, at a current density of 50 $mA\,g^{-1}$, the discharge capacity is ≈1,000 $mAh\,g^{-1}$, whereas at a current density of 2000 $mA\,g^{-1}$, discharge capacity decreases to ≈750 $mAh\,g^{-1}$. When the current density is re-set to the original value after 60 cycles, the original discharge capacity is recovered and a slight increase to ≈1,100 $mAh\,g^{-1}$ is noted, indicating performance enhancing chemical/structural changes within the material that are still under investigation.[50–52] Furthermore, the stable cycle performance at higher rates indicates fast solid-state Li^+ ion diffusion and is indicative of a short diffusion path length and structural stability.[15]

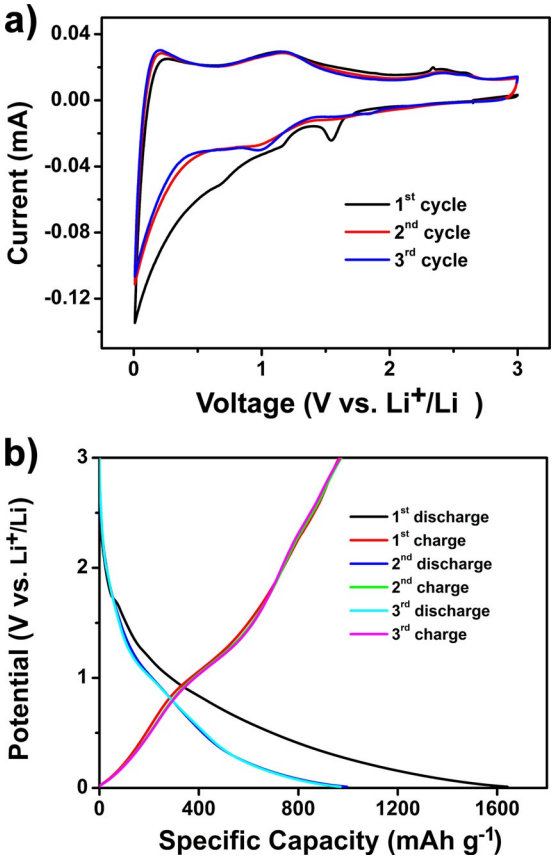

Figure 4. (a) Cyclic voltammograms of composite **1** (scan rate 0.1 $mV\,s^{-1}$) in the potential range 0.01–3 V vs. Li^+/Li. (b) The first three charging and discharging cycles of the LIB containing composite **1** at a current density of 100 $mA\,g^{-1}$. Note that the signal at 1.6 V in cycle 1 could be related to electrode or electrode–electrolyte redox processes and is still under investigation.

Electrochemical cycling of the battery is shown in Figure 5b and illustrates the cycling stability, specific capacity, and coulombic efficiency of composite **1** at a current density of 100 $mA\,g^{-1}$; after an initial drop (associated with SEI formation), the specific capacity reaches ca. 970 $mAh\,g^{-1}$ and remains stable for 100 cycles. In contrast, when tested under identical conditions at identical weight loadings, the precursors (GQDs, $\{MnV_{12}\}$) and a physical mixture of the components (obtained by grinding both components together) show significantly lower specific capacities (GQDs: 320 $mAh\,g^{-1}$, $\{MnV_{12}\}$: 560 $mAh\,g^{-1}$, physical mixture: 660 $mAh\,g^{-1}$). Examination of the coulombic efficiency shows that after an initial conditioning phase, a stable plateau at 99% efficiency is reached after 20 cycles and is retained for 1000 cycles (see the Supporting Information). Comparative analyses using an LIB anode fabricated with a higher active material content (weight ratio composite **1**: carbon black: poly(vinylidene fluoride = 80:10:10 showed a lower specific capacity after 100 cycles (750 $mAh\,g^{-1}$, −23% compared with the 50:40:10 electrode). The coulombic

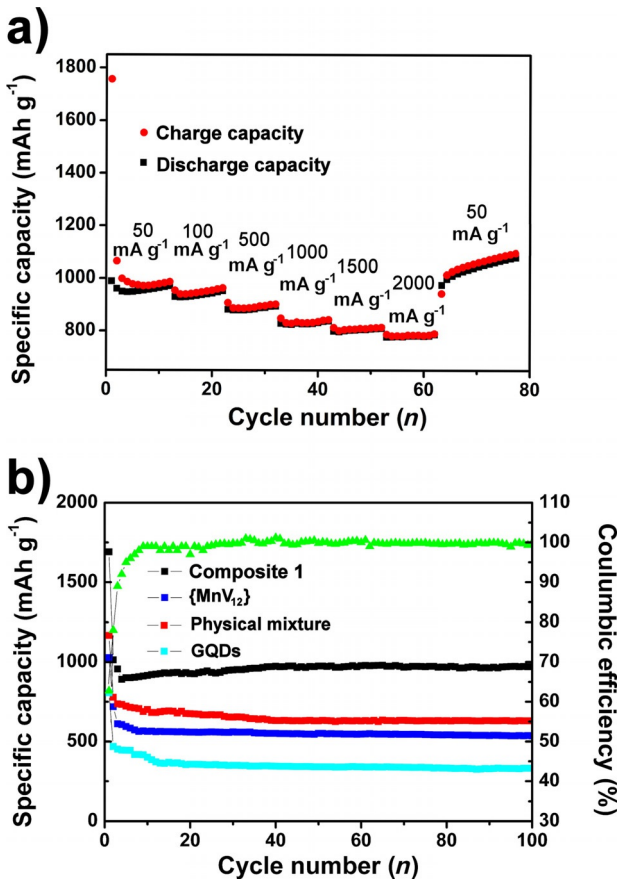

Figure 5. (a) Rate performance of composite **1** at current densities of 50 mA g^{-1} to 2000 mA g^{-1}, (b) specific discharge capacity and coulombic efficiency vs. cycle number for the precursors and composite **1** measured at a current density of 100 mA g^{-1}.

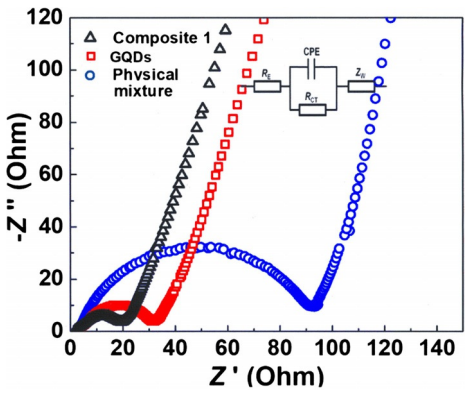

Figure 6. Nyquist plots of composite **1** as well as the physical component mixture and the pure GQDs used as anode material in an LIB. Inset: The simulated equivalent circuit of the electrode/electrolyte interface used to examine the composite. R_E: electrolyte resistance, R_{CT}: charge-transfer resistance, Z_w: Warburg impedance, CPE: constant-phase element.

Table 1. Comparison of specific capacities reported for manganese vanadium oxide anodes.

Material	Current density [mA g^{-1}]	Discharge capacity [mAh g^{-1}]	Ref.
MnV_2O_6	200	768	[38]
MnV_2O_6	50	600	[39]
$Mn_{1.5}(H_2O)(NH_4)V_4O_{12}$	100	980	[40]
$LiVO_{4-\delta}$	100	340	[53]
$Li_5MnV_2O_6$	100	500	[54]
Composite **1**	100	970	This work

efficiency was ca. 100% and no loss of activity was noted over 100 cycles, see the Supporting Information for details.

The sheet resistance of composite **1** was measured to be $1.9\times10^2\ \Omega\,cm^{-2}$, whereas the sheet resistance of GQDs and the physical mixture of **{MnV_{12}}** and GQDs were 3.1×10^2 and $8.2\times10^2\ \Omega\,cm^{-2}$, respectively. This finding is further supported by electrochemical impedance spectroscopy (EIS, see Figure 6), which showed lower charge transfer resistance (R_{CT}) and lower electrolyte resistance (R_E) compared to the reference compounds (for details, see the Supporting Information). In summary, this study illustrates that the sonication-driven assembly of GQDs and **{MnV_{12}}** clusters into graphene quantum dot/metal oxide nanocomposites results in a high-performance LIB anode material that combines electronic/ionic conductivity with high cycling stability. Comparison of the LIB anode performance of composite **1** with related manganese vanadium oxide systems is given in Table 1 and illustrates that **1** features promising specific capacity in addition with facile synthetic access and the use of earth-abundant, lightweight materials.

Conclusion

In conclusion, we report the facile one-step synthesis of a nanostructured graphene quantum dot (GQD)/manganese vanadate composite with well-defined rod-like morphology, which shows excellent performance as anode material in lithium ion batteries. High specific discharge capacities of ≈970 mAh g^{-1} are observed together with coulombic efficiencies near 100% over one hundred electrochemical cycles. It is further shown that the sonication-driven materials assembly is critical and leads to significant improvements in battery performance compared to the pure precursors or a "simple" physical mixture of the precursors. Future work will expand this study and explore the incorporation of other redox-active 3d metals with a focus on cobalt and iron vanadates to identify the most promising materials for further development. Theoretical and experimental spectroscopic and electron microscopic studies on the GQD/metal oxide interface will further explore the molecular-level structural features and mode of linkage between metal oxide and graphene quantum dots.

Experimental Section

Materials: All reagents were obtained from Sigma Aldrich, ABCR or ACROS and were of reagent grade. The chemicals were used without further purification unless stated otherwise. Graphene quantum dots (GQDs) were prepared according to ref. [41]. (nBu$_4$N)$_3$(DMA)[(MnCl)$V_{12}O_{32}$Cl]·EtOAc (**{MnV_{12}}**) was prepared according to ref. [36].

Preparation of composite 1: **{MnV_{12}}**[36] and GQDs[41] were synthesized according to published procedures. The composite is formed by mixing an aqueous suspension of GQDs (10 mL, 30 g L^{-1}) and an acetonitrile solution of **{MnV_{12}}** (20 mL, 1.0 mM). The resulting mixture was sonicated (300 W, 45 kHz) for 12 h at room temperature. The composite was isolated by centrifugation and washed three times with ethanol. The final product was obtained by drying in a vacuum oven at 40 °C overnight. Yield: ca. 93 wt.%.

Acknowledgements

Y.J. and C.S. acknowledge financial support by the Deutscher Akademischer Austauschdienst DAAD, Deutsche Forschungsgemeinschaft DFG (STR1164/4, STR1164/12), EU COST Action CM1203, and Ulm University. Y.-F.S. acknowledges financial support by the National Basic Research Program of China (973 program, 2014CB932104) and National Nature Science Foundation of China (U1407127, U1507102, 21521005, 21625101). Professor Maximilian Fichtner (Helmholtz-Institute Ulm) is gratefully acknowledged for helpful discussions and instrument access.

Conflict of interest

The authors declare no conflict of interest.

Keywords: composites · electrochemistry · metal oxide nanoparticles · polyoxometalates · self-assembly

[1] N. Nitta, F. Wu, J. T. Lee, G. Yushin, *Mater. Today* **2015**, *18*, 252 – 264.
[2] P. Poizot, S. Laruelle, S. Grugeon, L. Dupont, J. M. Tarascon, *Nature* **2000**, *407*, 496 – 499.
[3] J. C. Bachman, S. Muy, A. Grimaud, H. Chang, N. Pour, S. F. Lux, O. Paschos, F. Maglia, S. Lupart, P. Lamp, L. Giordano, Y. Shao-Horn, *Chem. Rev.* **2016**, *116*, 140 – 162.
[4] Y. Ji, L. Huang, J. Hu, C. Streb, Y.-F. Song, *Energy Environ. Sci.* **2015**, *8*, 776 – 789.
[5] H. Wang, L.-F. Cui, Y. Yang, H. Sanchez Casalongue, J. T. Robinson, Y. Liang, Y. Cui, H. Dai, *J. Am. Chem. Soc.* **2010**, *132*, 13978 – 13980.
[6] M. V. Reddy, G. V Subba Rao, B. V. R. Chowdari, *Chem. Rev.* **2013**, *113*, 5364 – 5457.
[7] Y. Zhao, L. P. Wang, M. T. Sougrati, Z. Feng, Y. Leconte, A. Fisher, M. Srinivasan, Z. Xu, *Adv. Energy Mater.* **2017**, *7*, 1601424.
[8] Z. Wang, L. Zhou, X. W. (David) Lou, *Adv. Mater.* **2012**, *24*, 1903 – 1911.
[9] S. Yang, X. Feng, S. Ivanovici, K. Müllen, *Angew. Chem.* **2010**, *122*, 8586 – 8589.
[10] For a special issue on polyoxometalate science, see: L. Cronin, A. Müller, *Chem. Soc. Rev.* **2012**, *41*, 7333 – 7334 and other manuscripts in the same issue.
[11] A. Proust, B. Matt, R. Villanneau, G. Guillemot, P. Gouzerh, G. Izzet, *Chem. Soc. Rev.* **2012**, *41*, 7605 – 7622.
[12] S. Herrmann, C. Ritchie, C. Streb, *Dalton Trans.* **2015**, *44*, 7092 – 7104.
[13] N. Kawasaki, H. Wang, R. Nakanishi, S. Hamanaka, R. Kitaura, H. Shinohara, T. Yokoyama, H. Yoshikawa, K. Awaga, *Angew. Chem. Int. Ed.* **2011**, *50*, 3471 – 3474; *Angew. Chem.* **2011**, *123*, 3533 – 3536.
[14] Y. Nishimoto, D. Yokogawa, H. Yoshikawa, K. Awaga, S. Irle, *J. Am. Chem. Soc.* **2014**, *136*, 9042 – 9052.
[15] Y. Ji, J. Hu, L. Huang, W. Chen, C. Streb, Y.-F. Song, *Chem. Eur. J.* **2015**, *21*, 6469 – 6474.
[16] J. Hu, Y. Ji, W. Chen, C. Streb, Y.-F. Song, *Energy Environ. Sci.* **2016**, *9*, 1095 – 1101.
[17] C. Streb, *Structure and Bonding in Molecular Vanadium Oxides: From Templates via Host-Guest Chemistry to Applications in Structure and Bonding*, Springer, Berlin, Heidelberg, **2017**.
[18] M. Anjass, K. Kastner, F. Naegele, M. Ringenberg, J. Boas, J. Zhang, A. Bond, T. Jacob, C. Streb, *Angew. Chem. Int. Ed.* **2017**, *56*, 14754 – 14757; *Angew. Chem.* **2017**, *129*, 14949 – 14952.
[19] J.-J. Chen, M. D. Symes, S.-C. Fan, M.-S. Zheng, H. N. Miras, Q.-F. Dong, L. Cronin, *Adv. Mater.* **2015**, *27*, 4649 – 4654.
[20] S. Hartung, N. Bucher, H.-Y. Chen, R. Al-Oweini, S. Sreejith, P. Borah, Z. Yanli, U. Kortz, U. Stimming, H. E. Hoster, M. Srinivasan, *J. Power Sources* **2015**, *288*, 270 – 277.
[21] H.-Y. Chen, J. Friedl, C.-J. Pan, A. Haider, R. Al-Oweini, Y. L. Cheah, M.-H. Lin, U. Kortz, B.-J. Hwang, M. Srinivasan, U. Stimming, *Phys. Chem. Chem. Phys.* **2017**, *19*, 3358 – 3365.
[22] J. W. Choi, D. Aurbach, *Nat. Rev. Mater.* **2016**, *1*, 16013.
[23] W. Luo, J. Hu, H. Diao, B. Schwarz, C. Streb, Y.-F. Song, *Angew. Chem. Int. Ed.* **2017**, *56*, 4941 – 4944; *Angew. Chem.* **2017**, *129*, 5023 – 5026.
[24] C. Streb, R. Tsunashima, D. A. MacLaren, T. McGlone, T. Akutagawa, T. Nakamura, A. Scandurra, B. Pignataro, N. Gadegaard, L. Cronin, *Angew. Chem. Int. Ed.* **2009**, *48*, 6490 – 6493; *Angew. Chem.* **2009**, *121*, 6612 – 6615.
[25] J. Livage, *Chem. Mater.* **1991**, *3*, 578 – 593.
[26] L. A. Ponomarenko, F. Schedin, M. I. Katsnelson, R. Yang, E. W. Hill, K. S. Novoselov, A. K. Geim, *Science* **2008**, *320*, 356 – 358.
[27] Z. Zhang, J. Zhang, N. Chen, L. Qu, *Energy Environ. Sci.* **2012**, *5*, 8869 – 8890.
[28] Y. P. Sun, B. Zhou, Y. Lin, W. Wang, K. A. S. Fernando, P. Pathak, M. J. Meziani, B. A. Harruff, X. Wang, H. Wang, P. G. Luo, H. Yang, M. E. Kose, B. Chen, L. M. Veca, S. Y. Xie, *J. Am. Chem. Soc.* **2006**, *128*, 7756 – 7757.
[29] Y. Dong, H. Pang, H. Bin Yang, C. Guo, J. Shao, Y. Chi, C. M. Li, T. Yu, *Angew. Chem. Int. Ed.* **2013**, *52*, 7800 – 7804; *Angew. Chem.* **2013**, *125*, 7954 – 7958.
[30] L. Cao, X. Wang, M. J. Meziani, F. Lu, H. Wang, P. G. Luo, Y. Lin, B. A. Harruff, L. M. Veca, D. Murray, S. Xie, Y. Sun, *J. Am. Chem. Soc.* **2007**, *129*, 11318 – 11319.
[31] K. Ritter, J. Lyding, *Nat. Mater.* **2009**, *8*, 235 – 242.
[32] D. Pan, J. Zhang, Z. Li, M. Wu, *Adv. Mater.* **2010**, *22*, 734 – 738.
[33] G. Konstantatos, M. Badioli, L. Gaudreau, J. Osmond, M. Bernechea, F. P. G. de Arquer, F. Gatti, F. H. L. Koppens, *Nat. Nanotechnol.* **2012**, *7*, 363 – 368.
[34] C. Zhu, D. Chao, J. Sun, I. M. Bacho, Z. Fan, C. F. Ng, X. Xia, H. Huang, H. Zhang, Z. X. Shen, G. Ding, H. J. Fan, *Adv. Mater. Interfaces* **2015**, *2*, 1400499.
[35] J. Park, J. Moon, C. Kim, J. H. Kang, E. Lim, J. Park, K. J. Lee, S.-H. Yu, J.-H. Seo, J. Lee, J. Heo, N. Tanaka, S.-P. Cho, J. Pyun, J. Cabana, B. H. Hong, Y.-E. Sung, *NPG Asia Mater.* **2016**, *8*, e272.
[36] K. Kastner, J. T. Margraf, T. Clark, C. Streb, *Chem. Eur. J.* **2014**, *20*, 12269 – 12273.
[37] K. Kastner, J. Forster, H. Ida, G. N. Newton, H. Oshio, C. Streb, *Chem. Eur. J.* **2015**, *21*, 7686 – 7689.
[38] D. Deng, Y. Zhang, G. Li, X. Wang, L. H. Gan, L. Jiang, C. R. Wang, *Chem. Asian J.* **2014**, *9*, 1265 – 1269.
[39] T. Morishita, K. Nomura, T. Inamasu, M. Inagaki, *Solid State Ionics* **2005**, *176*, 2235 – 2241.
[40] M. K. Dufficy, L. Luo, P. S. Fedkiw, P. Maggard, *Chem. Commun.* **2016**, *52*, 7509 – 7512.
[41] D. Qu, M. Zheng, L. Zhang, H. Zhao, Z. Xie, X. Jing, R. E. Haddad, H. Fan, Z. Sun, *Sci. Rep.* **2014**, *4*, 5294.
[42] J. N. Coleman, *Acc. Chem. Res.* **2013**, *46*, 14 – 22.
[43] S. Laurent, D. Forge, M. Port, A. Roch, C. Robic, L. Vander Elst, R. N. Muller, *Chem. Rev.* **2008**, *108*, 2064 – 2110.
[44] S. Schönweiz, S. A. Rommel, J. Kübel, M. Micheel, B. Dietzek, S. Rau, C. Streb, *Chem. Eur. J.* **2016**, *22*, 12002 – 12005.
[45] K. Heussner, N. Rockstroh, K. Peuntinger, L. C. Nye, I. Ivanovic-Burmazovic, S. Rau, C. Streb, *Chem. Commun.* **2011**, *47*, 6852 – 6854.
[46] L. Huang, J. Hu, Y. Ji, C. Streb, Y.-F. Song, *Chem. Eur. J.* **2015**, *21*, 18799 – 18804.
[47] Y. Dou, J. Xu, B. Ruan, Q. Liu, Y. Pan, Z. Sun, S. X. Dou, *Adv. Energy Mater.* **2016**, *6*, 1501835.
[48] T. Morishita, H. Konno, Y. Izumi, M. Inagaki, *Solid State Ionics* **2006**, *177*, 1347 – 1353.
[49] D. Wang, Q. Wei, J. Sheng, P. Hu, M. Yan, R. Sun, X. Xu, Q. An, L. Mai, *Phys. Chem. Chem. Phys.* **2016**, *18*, 12074 – 12079.

[50] D. Bresser, E. Paillard, R. Kloepsch, S. Krueger, M. Fiedler, R. Schmitz, D. Baither, M. Winter, S. Passerini, *Adv. Energy Mater.* **2013**, *3*, 513 – 523.
[51] X. Wei, C. Tang, X. Wang, L. Zhou, Q. Wei, M. Yan, J. Sheng, P. Hu, B. Wang, L. Mai, *ACS Appl. Mater. Interfaces* **2015**, *7*, 26572 – 26578.
[52] L. Hou, L. Lian, L. Zhang, G. Pang, C. Yuan, X. Zhang, *Adv. Funct. Mater.* **2015**, *25*, 238 – 246.
[53] L. Chen, X. Jiang, N. Wang, J. Yue, Y. Qian, J. Yang, *Adv. Sci.* **2015**, *2*, 1500090.
[54] M. Simões, Y. Surace, S. Yoon, C. Battaglia, S. Pokrant, A. Weidenkaff, *J. Power Sources* **2015**, *291*, 66 – 74.

Manuscript received: August 16, 2017
Accepted manuscript online: October 5, 2017
Version of record online: November 7, 2017